Journal of Materials Processing Tech. 288 (2021) 116845

Contents lists available at ScienceDirect

Journal of Materials Processing Tech.

journal homepage: www.elsevier.com/locate/jmatprotec

Interfacial metal/ceramic bonding mechanism for metallization of ceramics via cold spraying

Jiahao Qin[a,b], Qun Huang[b], Xin Wang[c], Xinkun Suo[b,*], Jiang Wang[a,*], Hua Li[b]

[a] State Key Laboratory of Advanced Special Steel, School of Materials Science and Engineering, Shanghai University, Shanghai 200444, China
[b] Key Laboratory of Marine Materials and Related Technologies, Zhejiang Key Laboratory of Marine Materials and Protective Technologies, Ningbo Institute of Materials Technology and Engineering, Cixi Institute of Biomedical Engineering, Ningbo Institute of Materials Technology and Engineering, Chinese Academy of Sciences, Ningbo 315201, China
[c] Ningbo Jiangbei Gofront Herong Electric Co. Ltd., Ningbo 315033, China

ARTICLE INFO

Associate Editor: M. Merklein

Keywords:
Amorphous
Bonding mechanism
Ceramic
Cold spraying
Metallization
Rupture

ABSTRACT

Metallization of ceramics is drawing more and more attention in industries. The mechanisms involving high bonding strength between cold sprayed metallic coatings and ceramic substrates are not yet clear. In this study, aluminum (Al) particles and alumina (Al_2O_3) substrates were employed to reveal impact phenomena in cold spraying. Electron backscatter diffraction equipment (EBSD) and high-resolution transmission electron microscope (HRTEM) were used to investigate the interfacial microstructures of the Al particles and Al_2O_3 substrates. Computational fluid dynamics (CFD) and finite element analysis (FEA) were employed to quantitatively characterize the temperatures and plastic strains at the interfaces. The bonding strength of the Al coatings and Al_2O_3 substrates was measured and the analysis to the fracture morphologies was also conducted. The results show that the Al particles at the interfaces presented fine-grain and amorphous structures, and the Al_2O_3 substrates experienced a brittle rupture. The Al coatings bonded on the ceramic surfaces due to mechanical interlocking and heteroepitaxy. The results offer more details to understand the bonding mechanisms of metallic particles and ceramic substrates.

1. Introduction

Metallization of ceramic materials has become an important issue for their use in electronic information industries due to their excellent thermal conductivity, high-temperature insulation, and low dielectric constant (Belyakov et al., 2012). Kosarev et al. (2018) reported the Al_2O_3 and AlN ceramics coated with cold-sprayed Cu coatings, which can withstand more than 100 thermal cycles in a temperature ranged from -60 to +150 °C. Many kinds of technologies are employed to realize the metallization of ceramic materials. For example, Morita et al. (1991) utilized laser-sublimating and electroless plating to deposit thin metallic layers on AlN substrates to repair or customize circuits. Song et al. (2019) used direct bonding to deposit AgCuTi metallic layers on SiC ceramics to bond GH99 superalloys and ceramics. It is worth noted that the new phase TiC was observed between AgCuTi metallic layers and SiC ceramics, which was regarded as the product of chemical bonding. Reboun et al. (2017) employed silk-screen printing to fabricate thick copper films on alumina for power electronic industries. The average adhesion strength of the copper film was 43 MPa. Ritter et al. (2017) investigated the high temperature co-fired ceramic technology for ceramic sensors, in which the platinum heater and self-heated yttria-stabilized zirconia disc were bonded. Brust et al. (2016) applied physical vapour deposition and chemical vapour deposition to fabricate Ti and TiN thin films on Al_2O_3 and ZrO_2, respectively, to improve the wettability of filler materials on ceramics.

Cold spraying is a relatively new ceramic metallization technology, in which a high-temperature and high-pressure gas obtains a high velocity through an energy transformation in a De Laval nozzle; particles are accelerated to high velocities (300 − 1500 m/s) by the gas, and impact onto a substrate and form a coating in a solid-state (Assadi et al., 2016). Compared to the coatings fabricated using other metallization processes, cold sprayed coatings have higher purity and lower oxidation due to the low temperature characterization of cold spraying (Smith, 2007).

Cold spraying can be used to metallize ceramics, in which aluminum (Al), titanium (Ti) and copper (Cu) coatings were used as the coating materials, and alumina (Al_2O_3), aluminum nitride (AlN), silicon nitride (Si_3N_4), silicon carbide (SiC), magnesium fluoride (MgF_2), lead

* Corresponding authors.
E-mail addresses: suoxinkun@nimte.ac.cn (X. Suo), jiangwang@i.shu.edu.cn (J. Wang).

https://doi.org/10.1016/j.jmatprotec.2020.116845
Received 22 May 2020; Received in revised form 6 July 2020; Accepted 18 July 2020
Available online 25 July 2020

zirconate titanate (PZT) and zirconia (ZrO_2) were employed as the substrates. Ko et al. (2016) reported the amorphization and atomic intermixing phenomena at the interface of Cu/AlN and Al/ZrO_2 bonding couples. The authors attributed bonding between metal and ceramic to chemical adhesion. Wüstefeld et al. (2017) reported local heteroepitaxial growth phenomena in the bonding couple of Al/AlN. Local heteroepitaxy between Al and AlN was attributed to the increase of the substrate temperature and the recrystallization or melting of Al coatings. However, the heteroepitaxial growth was not found for other ceramics. Drehmann et al. (2018) attributed the bonding to mechanical interlocking in several bonding couples, e.g. Al/SiC, Al/Si_3N_4, Al/MgF_2. Kromer et al. (2018) pre-treated rough surfaces on SiC and Al_2O_3 ceramics using laser surface texturing before cold spraying, which promoted mechanical anchoring between metal and ceramic. In addition, King et al. (2010) reported that mechanical adhesion took place by penetrating aluminium into the open pores on the smooth PZT substrates. Another interesting issue should be noted that the bonding strength of the metallic coatings on these ceramics did not present quite different no matter whether the heteroepitaxial growth phenomenon was reported or not. This suggests that the bonding mechanisms between metallic coatings and ceramic substrates are still not clearly understood.

Therefore, in this investigation, Al particles were deposited on Al_2O_3 ceramics to form coatings using cold spraying. The microstructure evolution of the Al particles was characterized and simulated during impact. More detailed inspections to the interfaces of the coatings and substrates were conducted using EBSD and HRTEM. The bonding mechanisms of the Al coatings on the Al_2O_3 substrates were discussed.

2. Experiment details

2.1. Feedstock and equipment

A commercial pure Al powder (Changsha Tianjiu Metal Materials Co. Ltd, Changsha, China) was employed as feedstock. The morphology of the particles was characterized using a scanning electron microscope (FESEM, Quanta FEG250, FEI, Hillsboro, USA), and the particles presented a spherical shape (Fig. 1a). The particle size distribution of the powder was measured using a laser granularity analyzer (S3500-special, Microtrac, Montgomeryville, USA), and the average diameter of the particles was 69 μm (Fig. 1b). The Al_2O_3 ceramic plates (Yunyi Electronics Co. Ltd, Guangzhou, China) with a dimension of 25 mm × 20 mm × 1 mm were used as substrates. The surface morphology of Al_2O_3 ceramic plate was shown in Fig. 1c. The substrates were cleaned using alcohol in ultrasonic for ten minutes before spraying.

A commercial cold spray equipment (Kinetics 3000, Cold Gas Technology GmbH, Ampfing, Germany) was employed. Nitrogen was used as propelling and delivering powder gas. The pressure and temperature of the gas were 2.2 MPa and 300 °C, respectively. The standoff distance of the nozzle was set as 30 mm. The traverse speed of the nozzle was 0.05 m/s.

2.2. Characterizations on microstructures and bonding strength of coatings

The coatings for the microstructure observation were prepared through cutting, mounting, etching using Keller's reagent (95 % distilled water, 2.5 % HNO_3, 1.5 % HCl, 1 % HF in volume), respectively. The cross-sectional microstructures of the coatings and the morphologies of the single particles were characterized using FESEM. The cross-sectional microstructures of the single particles were observed using a dual-beam focused ion beam scanning electron microscope system (FIB-SEM, Helios-G4-CX, Thermo Scientific, Waltham, USA). The roughness profiles of the bonding interfaces (including the upper surfaces of the substrates and the under surfaces of the coatings) were measured via a white light interferometer (3D Optical Profilometer, UP-Lambda2, Rtec Instruments, San Jose, USA). The grain size and distribution of the coatings at the interfaces were evaluated using a scanning electron microscope (SEM, Verios G4 UC, Thermo Scientific, Waltham, USA) equipped with an electron backscatter diffraction probe (EBSD, Symmetry, Oxford Instruments, Oxford, UK). The coatings were pre-treated using a precision ion polishing system (PIPS, LEICA EM TIC3X, Leica Microsystems, Wetzlar, Germany). The lattice structures of the Al and Al_2O_3 at the interface were investigated using a high-resolution transmission electron microscope (HRTEM, Tecnai G2 F20 S-TWIN, FEI, Hillsboro, USA). The TEM photos were taken at the center of the metal-ceramic interface using the FIB-SEM.

The bonding strength between coatings and substrates was measured according to ASTM-C663-01 using a mechanical testing machine (SANS, CMT5105, MTS Industrial System Co. Ltd, Shenzhen, China). The testing was carried out with a drawing velocity of 1 mm/min and a load of 100 kN. Five samples were measured for each testing to ensure the repeatability of the values.

2.3. Numerical models and methodology

A commercially available finite element analysis software (ABAQUS, Version 6.14) was employed to investigate the impact behavior of the Al particle on the Al_2O_3 substrate. The Eulerian approach was employed because of its great ability to capture the real deformation features inside the coating. The numerical model with a meshing resolution of 1/50 d_p (mesh size of 0.4 μm) is shown in Fig. 2a. The diameter of the particle was set as 20 μm. The surface profile of the substrate was captured by the white light interferometer. Then the roughness data was transformed into the geometric model by the Gwyddion (Version 2.30), the Origin Pro (Version 2017C) and the Rhino (Version 6.7). Finally, the geometric model of the rough substrate was imported into Abaqus (Version 6.14). The morphology of the surface in the simulation is related to the surface in Fig. 1c. The meshing was carried out using the 3D Eulerian eight-node elements (EC3D8RT). The boundary conditions of the model were shown in Fig. 2b.

The linear elastic and Johnson-Cook constitutive models were

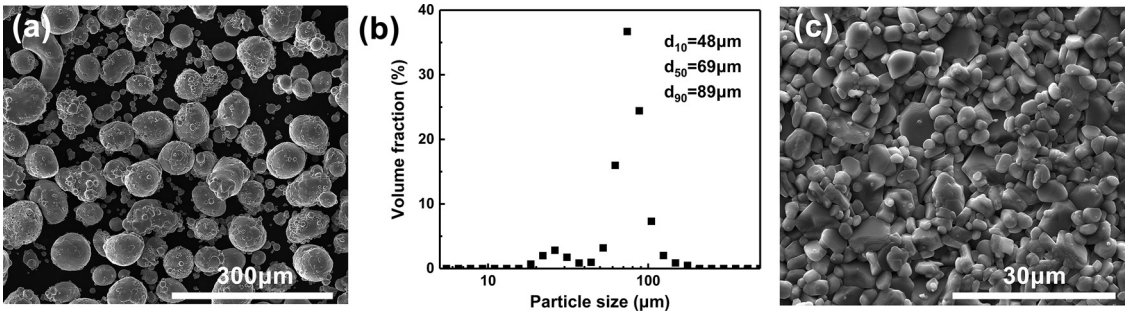

Fig. 1. The morphology (a), particle size distribution (b) of Al powder, and the morphology of Al_2O_3 ceramic plate (c).

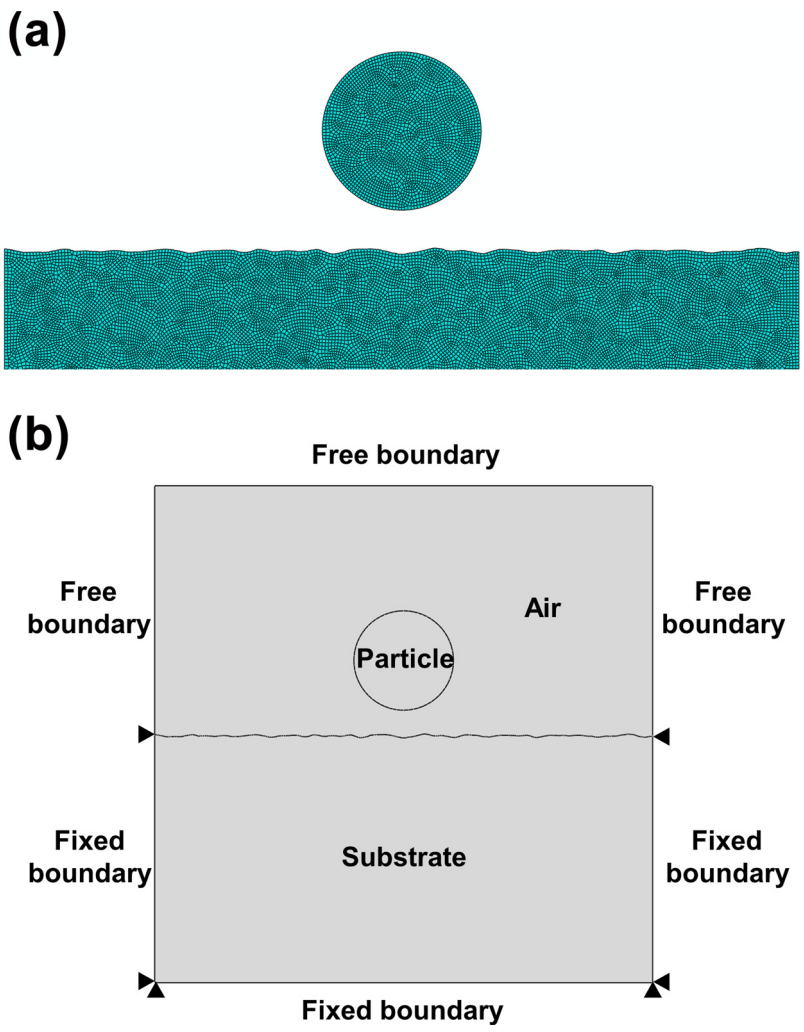

Fig. 2. The mesh (a) and boundary conditions (b) of Al particles impacting to Al_2O_3 substrates.

Table 1
Properties of Al and Al_2O_3 used in simulation.

Properties	Aluminum	Alumina
Density, ρ (kg/m^3)	2700	3890
Shear modulus, G (GPa)	26.2	–
Elastic modulus, E (GPa)	68.9	350
Poisson's ratio, ν	0.33	0.22
Specific heat, C_p (J/(kg K))	904	955
Thermal conductivity, λ (W/(m °C)	220	30
Yield strength, A (MPa)	148	–
Hardening coefficient, B (MPa)	345	–
Strain hardening exponent, N	0.183	–
Strain rate constant, C	0.001	–
Softening exponent, M	0.895	–
Melting temperature, Tm (K)	916	–
Reference temperature, T_0 (K)	298	–
Reference strain rate (s^{-1})	1	–
Sound velocity, C_0 (m/s)	5350	–
Slope in v_s versus v_p, S	1.37	–
Grüneisen coefficient, γ_0	2.14	–

employed for the ceramic substrate and Al particle, respectively. Kromer et al. (2018) used the linear elastic model to simulate the impact between the metallic particles and ceramic substrates, and the fracture of the ceramic substrate was also found in the figure. The parameters of the constitutive models were listed in Table 1. The velocity and temperature of particles were obtained from the computational fluid dynamics software (CFD, Ansys-Fluent, Version 16.0), which were set as 630 m/s and 401 K, respectively. These parameters were applied in the simulation of the single particle impact. The details of the CFD model can be found in the literature (Suo et al., 2015).

3. Results and discussion

3.1. Microstructure characterizations of the coatings

The cross-sectional microstructures of the Al particle and coating are shown in Fig. 3. No void, gap or other defect was observed in the coating and at the interface between the coating and substrate, indicating that the dense coating tightly bonded to the substrate. As etched by Keller's reagent, the boundaries of most particles were clearly observed, and there were also some boundaries disappeared (marked by the red arrows in Fig. 3a), indicating that metallurgical bonding occurred locally and the bonding was in a good condition. As illustrated in Fig. 3b, the deposited single particle exhibited the critical characteristics of cold spraying, including the fractures and jets at the edge of the particle (marked by the red circle), indicating that severe plastic deformation of the Al particle occurred during impact. Another interesting issue was that no jetting was found at the interface of the bonding (shown in Fig. 3c and d). Schmidt et al. (2006) held the opinion that the jet was an important criterion for metal-metal bonding in cold spraying. However, the story may be quite different in the metal-ceramic bonding. Jetting was not observed in the Fig. 3c and d, meanwhile it was observed in Fig. 3b. Thus, the jet was not the criterion for the

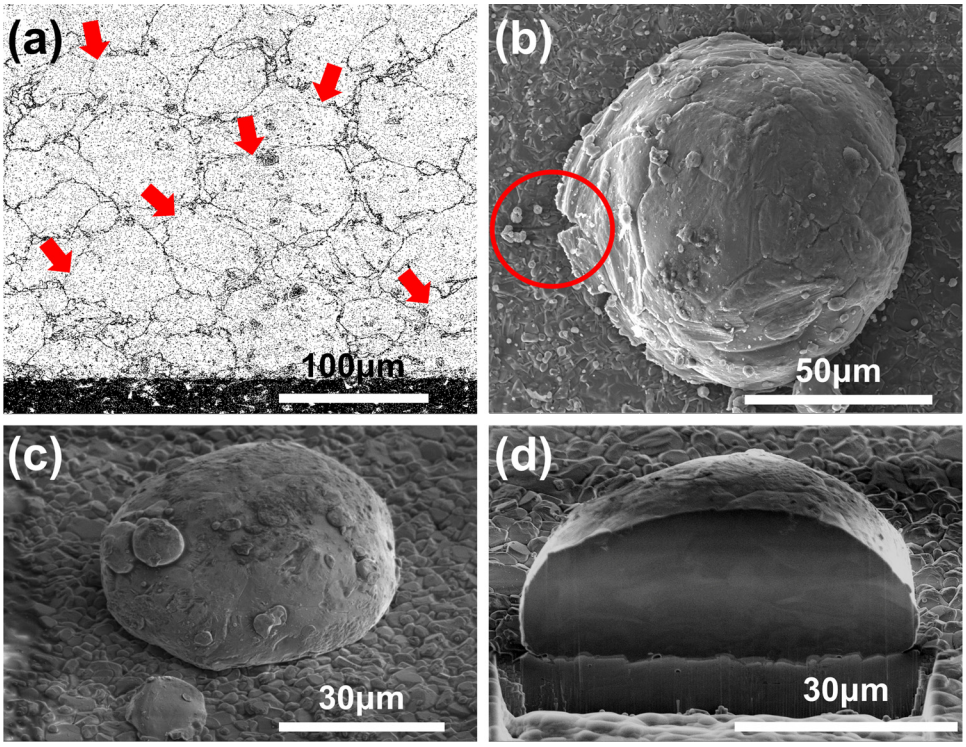

Fig. 3. The cross-sectional microstructures of Al coatings (a), surface morphologies of single particles (b, c) and cross-sectional microstructure of single Al particle (d) on Al_2O_3 substrates.

metal-ceramic bonding.

The evolution of the grains at the bonding interface is shown in Fig. 4. Fig. 4a shows the orientation map with respect to z-direction, and Fig. 4b is the partially enlarged drawing of Fig. 4a. The orientation map is usually used to reveal the grain orientation and size. Here, the red, blue and green areas represent the different crystal directions of [001], [111] and [101], respectively. The deposited particle at the interface is marked by the red line (Fig. 4a). It can be found that the orientations of the grains were irregular at the interface. It can also be found that the grains at the interface decreased significantly, and the size of the refined grains was in a several microns (Fig. 4b). Drehmann et al. (2018) also reported the grain refinement phenomena in the metal-ceramic bonding, which was attributed to the recrystallization of the metal. Another recrystallization evidence is shown in Fig. 4c and d, which was recrystallized fraction mappings of the grains at the interface. Fig. 4d is the partially enlarged drawing of Fig. 4c. In the recrystallized fraction mappings, fully recrystallized grains are shown in blue, deformed regions in red and substructured (recrystallized with subgrains) grains in yellow. The grains at the interface presented the blue color, suggesting that recrystallization occurred during impact. Meanwhile, the mechanism of recrystallization was also explained by the numerical simulation. The impact temperature of the Al particle at the interface was simulated using FEA, and the result is shown in Fig. 5c. The result shows that the highest transient local temperature of the particle at the interface was 703 K. The recrystallization temperature of the Al particle was 420 K (0.45 T_m). Therefore, the calculated local temperature was higher than the recrystallization temperature of the particle, resulting in the dynamic recrystallization phenomena.

The lattice structures of the Al and Al_2O_3 at the interface were also investigated using HRTEM, in order to reveal the bonding phenomena of the Al and Al_2O_3 during impact. The result is shown in Fig. 6. Three kinds of areas with different lattice structures were found, marked using A, B, and C respectively in the figure. Zone A contains the $(11\bar{1})_{Al}$ (2.338 Å), $(111)_{Al}$ (2.338 Å) and $(00\bar{2})_{Al}$ (2.024 Å) crystal plane of the Al particle. Zone C was the $(\bar{1}14)_{alumina}$ (2.551 Å), $(102)_{alumina}$ (3.479 Å) and $(\bar{2}12)_{alumina}$ (2.234 Å) crystal plane of the Al_2O_3 substrate. It can be found that the lattice planes of $(11\bar{1})_{Al}$ and $(\bar{1}14)_{alumina}$ arranged with an angle, and the lattice mismatch coefficient of the lattice planes was −8.3 %. The lattice planes of $(00\bar{2})_{Al}$ and $(\bar{2}12)_{alumina}$ grew parallel with a lattice mismatch coefficient of −9.4 %. Wüstefeld et al. (2017) also reported the lattice mismatch phenomena of $(220)_{Al}$ and $(2\bar{1}0)_{AlN}$, in which the lattice mismatch coefficient was −7.9 %. They attributed the bonding between Al and AlN to heteroepitaxy. An amorphous layer of about 10 nm was verified using the Fast Fourier Transform pattern (FFT). The amorphous layer is marked as zone B. There were sharp boundaries between amorphous zone, Al and Al_2O_3 (marked by white and blue arrows in Fig. 6). Xiong et al. (2011) also reported the amorphization phenomenon at the Ni/Cu interface, which was attributed to the synergistic effects of rapid quenching and high strain rate deformation. Ko et al. (2016) reported an amorphous layer at the interfaces of Al/ZrO_2 and Cu/AlN, and attributed it to the high velocity collision cascades instead of mechanical interlocking. The amorphization involved atomic intermixing and chemical adhesion forces. Here, the formation mechanism of the amorphous phase during impact was also investigated through numerical simulation. The temperature and equivalent plastic distribution (PEEQ) of the Al coating at the interface during impact were 703 K and 8.622, respectively (Fig. 5a and c). The temperature of the Al particle impacting on the ceramic was higher than that impacted on the metallic substrate due to the lower thermal conductivity of the ceramic (Fig. 5c and d). The PEEQ was also higher than that for the ceramic substrate because of its higher hardness (Fig. 5a and b). Therefore, amorphization is attributed to the high strain rate deformation in this investigation.

Amorphization and heteroepitaxy were usually found synchronously in cold sprayed metal-ceramic bonding couples. Wüstefeld et al. (2017) pointed out the heteroepitaxy phenomenon between Al and AlN, but amorphization can also be found in this reference. Drehmann et al. (2018) designated the heteroepitaxy phenomenon between Al and Al_2O_3, but amorphization can also be found in this reference. Therefore, amorphization may be thought as the criterion of heteroepitaxy in cold

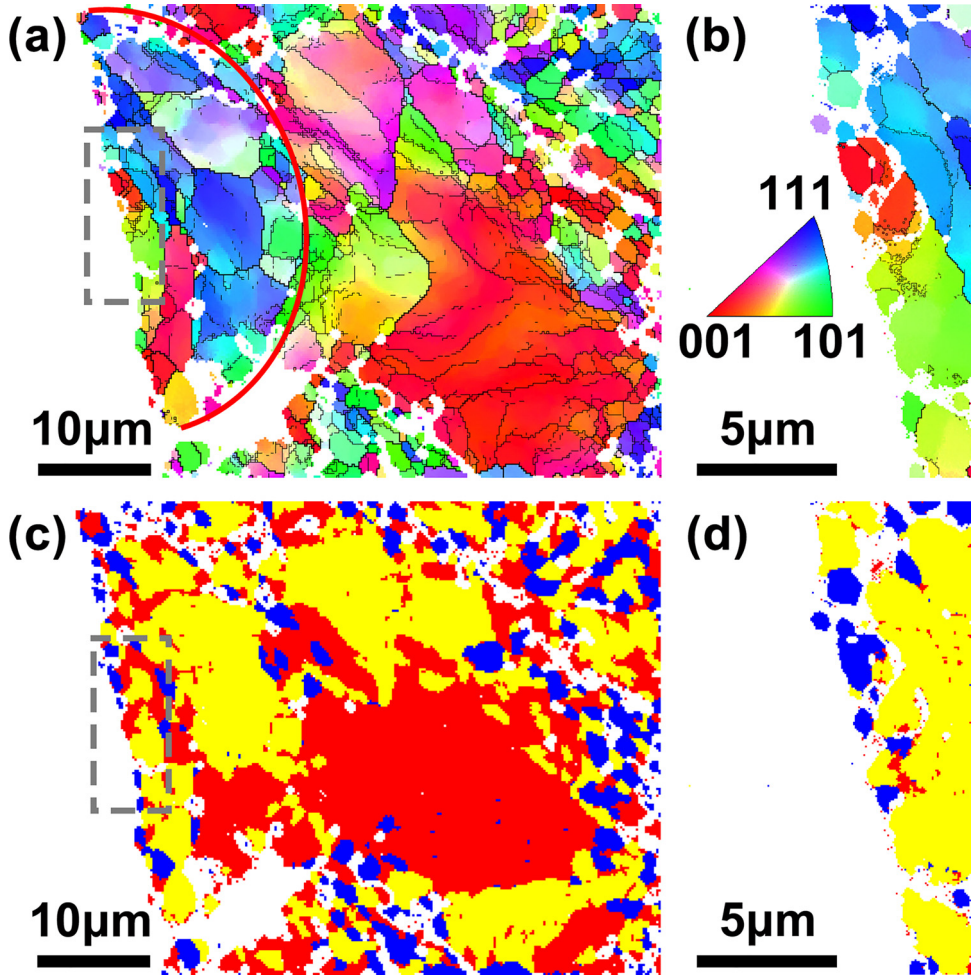

Fig. 4. The grain evolution of Al particle at the interfaces of coatings and substrates: orientation maps (a, b), recrystallized fraction mappings (c, d).

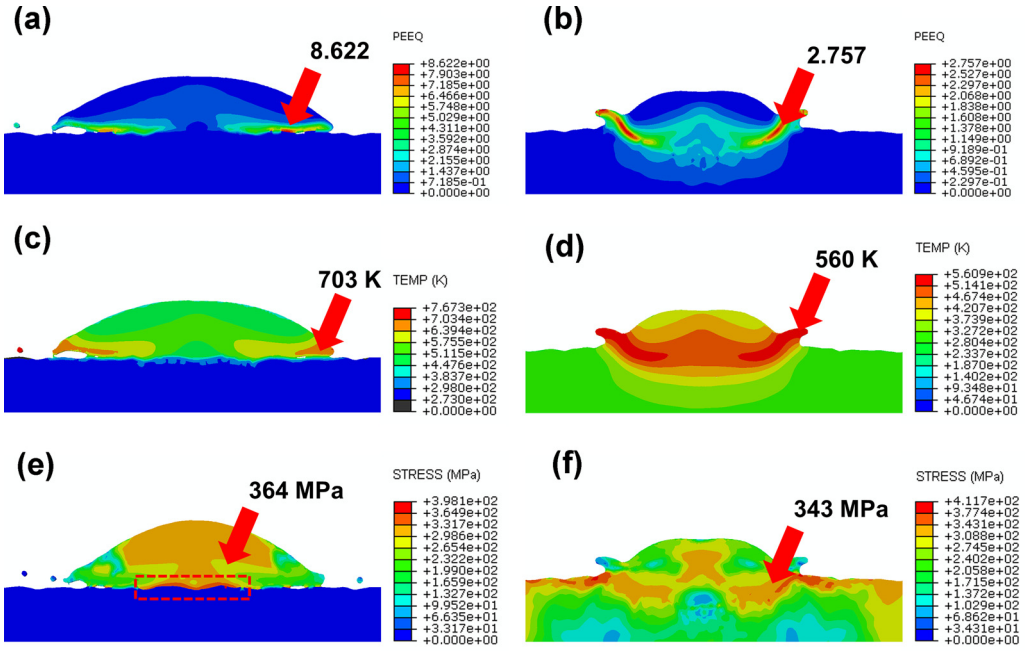

Fig. 5. The computational results of Al particles impacting to Al_2O_3 substrates and Al substrates: the PEEQ (a), temperature (c) and stress (e) of Al particles impacting to Al_2O_3 substrates; the PEEQ (b), temperature (d) and stress (f) of Al particles impacting to Al substrates.

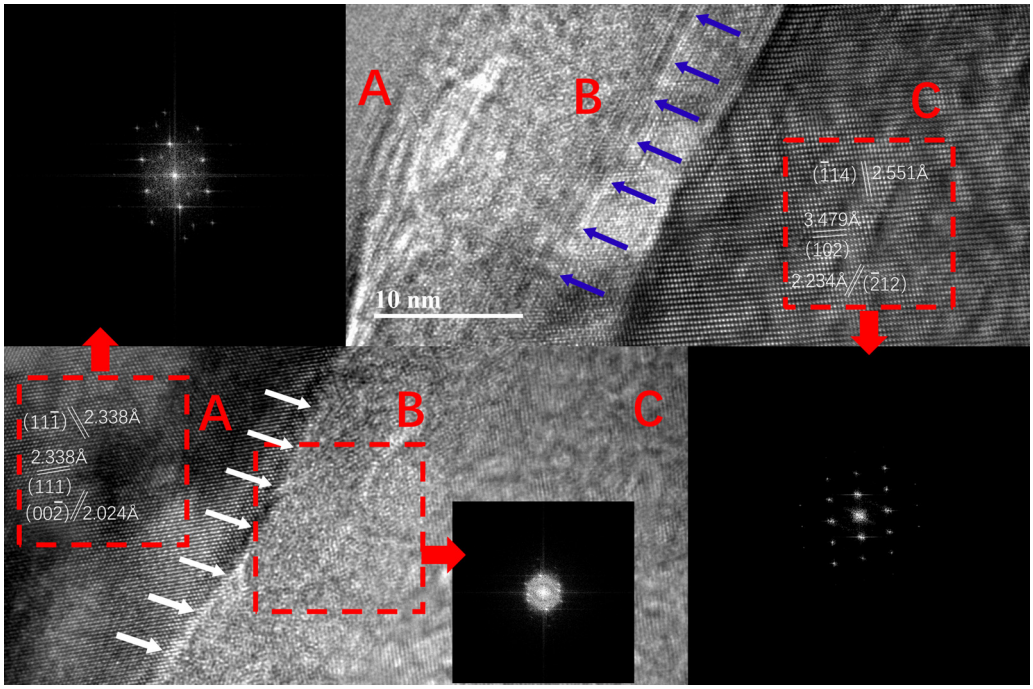

Fig. 6. HRTEM images of the interfaces of coatings and substrates.

sprayed metal-ceramic bonding couples.

3.2. Characterization of bonding strength and discussion of bonding mechanism

Fig. 7 shows the topographies of the under surface of the coating and the upper surface of the substrate after breaking the coating and substrate apart. It is found that the surface of the substrate presented some convex structures (Fig. 7a), and the under surface of the coating presented some concave structures (Fig. 7c). The concave-convex structures show similar size and distribution. The roughness of the surfaces was characterized using the white light interferometer. The result shows that the roughness of the coating and the substrate were 1.71 μm and 2.36 μm, respectively (Fig. 7b and d). Both morphology observation and roughness measurement reveal the matching of the under surface of the coating and the upper surface of the substrate, which can be thought as the evidence of mechanical bonding.

The bonding strength of the coatings was measured. The result shows that the average value of bonding strength was 29.6 ± 12.6 MPa. This value of the bonding strength was usually found for mechanical bonding. For example, Kromer et al. (2018) reported that the bonding strength of the Al coating and the rough Al_2O_3

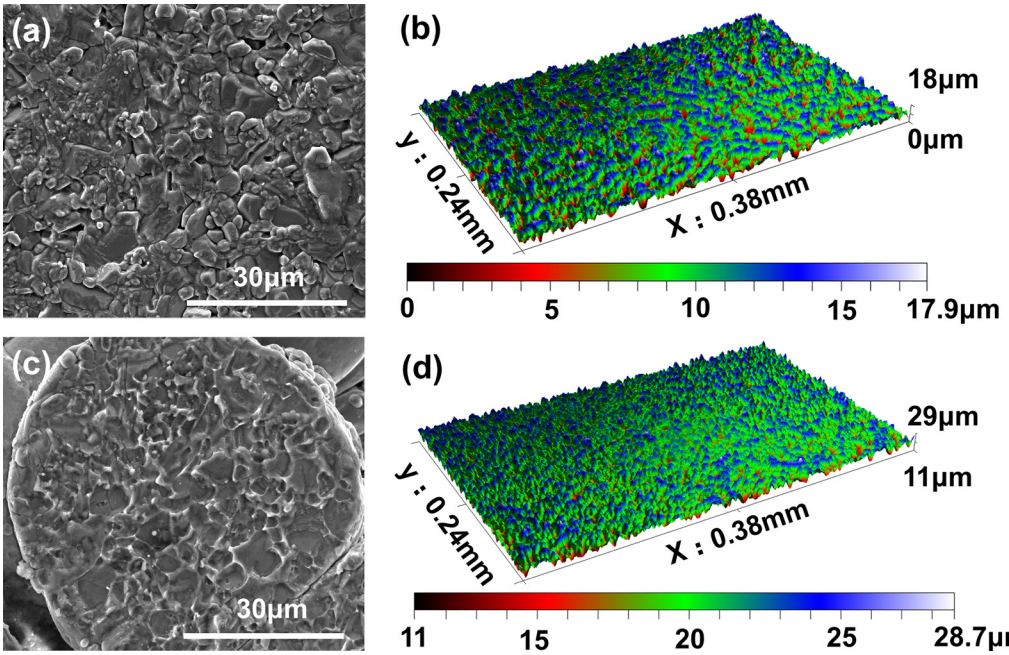

Fig. 7. The morphologies and roughness of Al coatings and Al_2O_3 substrates: the SEM image of Al_2O_3 surface (a), the 3D-profile image of Al_2O_3 surface (b), the SEM image of the under surface of the coating (c), the 3D-profile image of the under surface of the coating (d).

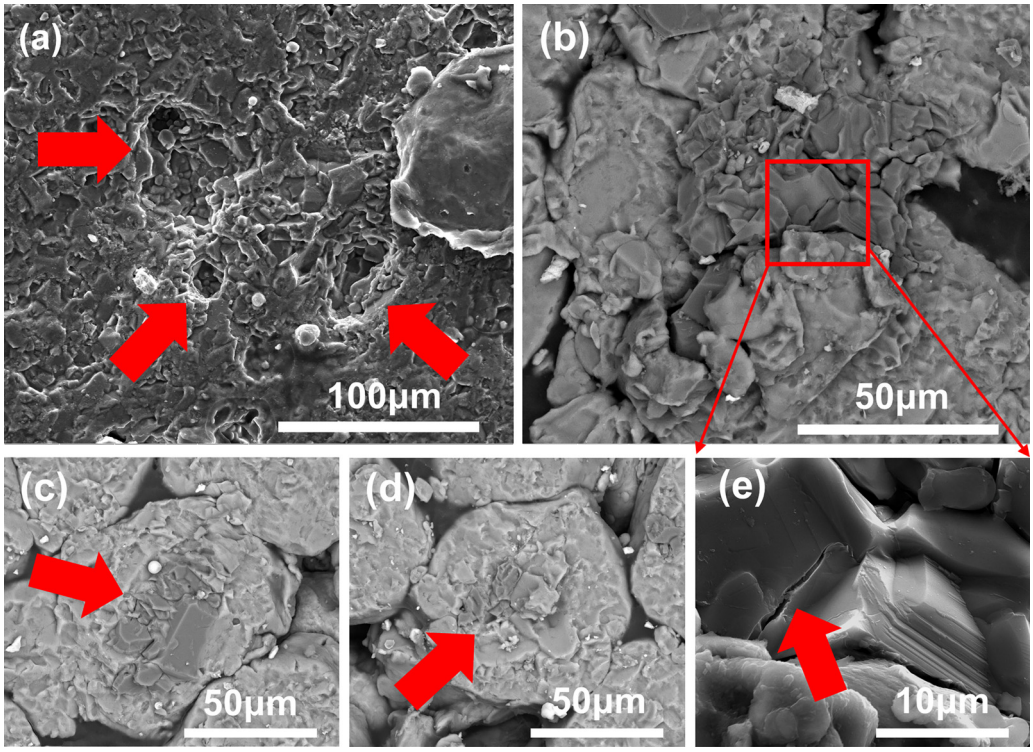

Fig. 8. The fracture morphologies of coatings and substrates after tensile testing: the SEM image of the substrate (a), the SEM images of Al_2O_3 debris on the coatings (b-d), the locally enlarged view of Fig.8b (e).

substrate was 20 MPa, demonstrating the function of the mechanical anchoring. Yang et al. (2014) reported the bonding strength of Cu/AISI304 was 22 MPa in plasma spraying, attributed to the mechanical bonding. It should also be noted that the bonding strength in this investigation was similar to other data although heteroepitaxy was reported in the literature (Drehmann et al., 2018). Therefore, the heteroepitaxy maybe not contribute to the improvement of bonding strength.

The fracture morphologies of the substrate and coating are shown in Fig. 8. Fig. 8a shows the fracture morphology of the substrate, Fig. 8b–d show the fracture morphologies of the coating, and Fig. 8e is the enlarged drawing of Fig. 8b. It is found that some pits occurred on the surface of the ceramic substrate (marked by red arrows in Fig. 8a). Meanwhile, some debris were found on the under surface of the coating, which was identified as Al_2O_3 debris (marked in Fig. 8b–d). This indicates that the material of the substrate transferred to the coating. The fracture was observed for the adhered ceramic on the coating (Fig. 8e), indicating that the ceramic was broken during the impact or tensile testing. The compressive stress of the Al particle impacting to the substrate was 364 MPa, calculated using FEA (Fig. 5e). The flexural strength of the commercial Al_2O_3 ceramic was 300 MPa, illuminated by the feedstock supplier. Therefore, the rupture of the Al_2O_3 occurred during the impact. Imbriglio et al. (2019) and King et al. (2010) also reported the reduced bonding strength, induced by the fracture in Ti/Al_2O_3 and Al/PZT bonding couples. Decreasing the particle velocity may avoid the fracture of the ceramic substrate. However, it will involve the low bonding strength between the Al coating and ceramic substrate. Another interesting phenomenon can be found in Fig. 8b–d. The ceramic debris were found to always adhere on the middle zone of the Al particle, suggesting that the Al particles imposed the highest impact forces to the substrates in the south pole regions of the particles.

4. Conclusion

Al and Al_2O_3 were employed to investigate the bonding mechanism of cold sprayed metallic coatings on ceramic substrates. The microstructures of the coatings and deposited single particles were characterized. The bonding strength of the Al particles and Al_2O_3 substrates were measured, and the fracture morphologies were analyzed. Main conclusion can be drawn.

(1) The Al coatings bonded on the ceramic surfaces due to mechanical interlocking and heteroepitaxy bonding, without jet as the bonding criterion. The under surfaces of the Al coatings copied the roughness of the ceramic's upper surfaces.
(2) Dynamic recrystallization and amorphization were found at the interfaces of metallic particles and ceramic substrates due to high strain rate deformation.
(3) The Al_2O_3 substrates were broken up due to the impact of the Al particles. The Al_2O_3 debris were peeled off from the substrates.

CRediT authorship contribution statement

Jiahao Qin: Methodology, Formal analysis, Writing - original draft. **Qun Huang:** Data curation, Software. **Xin Wang:** Visualization. **Xinkun Suo:** Conceptualization, Methodology, Writing - review & editing. **Jiang Wang:** Validation. **Hua Li:** Supervision.

Declaration of Competing Interest

The authors declare that they have no known competing financial interests or personal relationships that could have appeared to influence the work reported in this paper.

Acknowledgments

This work was supported by National Natural Science Foundation of China (21705158), Key Research and Development Program of Zhejiang Province (2015C01036), International Scientific and Technological Cooperation Project of Ningbo (2017D10011).

References

Assadi, H., Kreye, H., Gärtner, F., Klassen, T., 2016. Cold spraying – a materials perspective. Acta Mater. 116, 382–407. https://doi.org/10.1016/j.actamat.2016.06.034.

Belyakov, A.V., Kuznetsova, I.G., Kuftyrev, R.Y., Pilavova, L.V., Seregin, V.S., 2012. Metallization of aluminun nitride ceramic (Review). Glass Ceram. 69, 270–273. https://doi.org/10.1007/s10717-012-9460-y. English translation of Steklo i Keramika.

Brust, S., Röttger, A., Theisen, W., 2016. High-temperature stability and interfacial reactions of Ti and TiN thin films on Al_2O_3 and ZrO_2. Surf. Coat. Technol. 307, 47–55. https://doi.org/10.1016/j.surfcoat.2016.08.060.

Drehmann, R., Grund, T., Lampke, T., Wielage, B., Wüstefeld, C., Motylenko, M., Rafaja, D., 2018. Essential factors influencing the bonding strength of cold-sprayed aluminum coatings on ceramic substrates. J. Therm. Spray Technol. 27, 446–455. https://doi.org/10.1007/s11666-018-0688-0.

Imbriglio, S.I., Hassani-Gangaraj, M., Veysset, D., Aghasibeig, M., Gauvin, R., Nelson, K.A., Schuh, C.A., Chromik, R.R., 2019. Adhesion strength of titanium particles to alumina substrates: a combined cold spray and LIPIT study. Surf. Coat. Technol. 361, 403–412. https://doi.org/10.1016/j.surfcoat.2019.01.071.

King, P.C., Zahiri, S., Jahedi, M., Friend, J., 2010. Aluminium coating of lead zirconate titanate-a study of cold spray variables. Surf. Coat. Technol. 205, 2016–2022. https://doi.org/10.1016/j.surfcoat.2010.08.084.

Ko, K.H., Choi, J.O., Lee, H., 2016. The interfacial restructuring to amorphous: a new adhesion mechanism of cold-sprayed coatings. Mater. Lett. 175, 13–15. https://doi.org/10.1016/j.matlet.2016.03.132.

Kosarev, V.F., Klinkov, S.V., Melamed, B.M., Nepochatov, Y.K., Ryashin, N.S., Shikalov, V.S., 2018. Cold spraying for power electronics: deposition of thick topologically patterned copper layers on ceramics. AIP Conference Proceedings 2027. https://doi.org/10.1063/1.5065141.

Kromer, R., Danlos, Y., Costil, S., 2018. Cold gas-sprayed deposition of metallic coatings onto ceramic substrates using laser surface texturing pre-treatment. J. Therm. Spray Technol. 27, 809–817. https://doi.org/10.1007/s11666-018-0718-y.

Morita, N., Watanabe, T., Yoshida, Y., Nakagawa, T., 1991. Newly developed laser-sublimating method for direct formation of conductor film on ceramic substrates. CIRP Ann. – Manuf. Technol. 40, 191–193 https://doi.org /10.1016/S0007-8506(07)61965-61969.

Reboun, J., Hromadka, K., Hermansky, V., Johan, J., 2017. Properties of power electronic substrates based on thick printed copper technology. Microelectron. Eng. 167, 58–62. https://doi.org/10.1016/j.mee.2016.10.019.

Ritter, T., Hagen, G., Kita, J., Wiegärtner, S., Schubert, F., Moos, R., 2017. Self-heated HTCC-based ceramic disc for mixed potential sensors and for direct conversion sensors for automotive catalysts. Sens. Actuators B Chem. 248, 793–802. https://doi.org/10.1016/j.snb.2016.11.079.

Schmidt, T., Gärtner, F., Assadi, H., Kreye, H., 2006. Development of a generalized parameter window for cold spray deposition. Acta Mater. 54, 729–742. https://doi.org/10.1016/j.actamat.2005.10.005.

Smith, M.F., 2007. Comparing cold spray with thermal spray coating technologies. The Cold Spray Materials Deposition Process: Fundamentals and Applications 1911. pp. 43–61. https://doi.org/10.1533/9781845693787.1.43.

Song, Y., Liu, D., Hu, S., Song, X., Lei, Y., Cao, J., 2019. Brazing of metallized SiC ceramic to GH99 superalloy using graphene nanoplatelets reinforced AgCuTi composite filler. Ceram. Int. 45, 8962–8970. https://doi.org/10.1016/j.ceramint.2019.01.227.

Suo, X., Yin, S., Planche, M.P., Liu, T., Liao, H., 2015. Strong effect of carrier gas species on particle velocity during cold spray processes. Surf. Coat. Technol. 268, 90–93. https://doi.org/10.1016/j.surfcoat.2014.04.039.

Wüstefeld, C., Rafaja, D., Motylenko, M., Ullrich, C., Drehmann, R., Grund, T., Lampke, T., Wielage, B., 2017. Local heteroepitaxy as an adhesion mechanism in aluminium coatings cold gas sprayed on AlN substrates. Acta Mater. 128, 418–427. https://doi.org/10.1016/j.actamat.2017.02.021.

Xiong, Y., Xiong, X., Yoon, S., Bae, G., Lee, C., 2011. Dependence of bonding mechanisms of cold sprayed coatings on strain-rate-induced non-equilibrium phase transformation. J. Therm. Spray Technol. 20, 860–865. https://doi.org/10.1007/s11666-011-9634-0.

Yang, K., Liu, M., Deng, C., 2014. Adhesion strength of Cu coating on substrate at different temperatures. Surf. Eng. 30, 814–821. https://doi.org/10.1179/1743294414Y.0000000320.